Adaptive Robust Posture Control of Parallel Manipulator Driven by Pneumatic Muscles With Redundancy

Xiaocong Zhu, Guoliang Tao, Bin Yao, *Member, IEEE*, and Jian Cao

***Abstract*—This paper presents an adaptive robust posture controller for a parallel manipulator driven by pneumatic muscles (PMDPM) with a redundant DOF. Rather severe parametric uncertainties and uncertain nonlinearities exist in the dynamics of the PMDPM. To deal with these uncertainties effectively, the recently developed adaptive robust control strategy is applied. Furthermore, the developed control strategy explicitly takes into account the particular physical properties of the system studied. Specifically, the symmetric geometric structure of the parallel manipulator driven by identical pneumatic muscles and no external moments around symmetry-axis direction of the parallel manipulator make the rotation angle of the parallel manipulator around its symmetry axis direction negligible and a nonfactor during normal operations. As such, the axial rotation angle is not measured and controlled when the PMDPM are used in practice, leading to a single-DOF redundancy in synthesizing the precise posture controller for rotation angles around other axes. To make full use of this redundancy, an equivalent average-stiffness-like desired constraint is introduced in the development of the adaptive robust posture controller to achieve precise posture tracking while reducing control input chattering caused by measurement noise. Experimental results are obtained to verify the validity of the proposed controller for the redundant PMDPM.**

***Index Terms*—Adaptive robust control (ARC), parallel manipulator, pneumatic muscle, redundancy, uncertainties.**

I. Introduction

PNEUMATIC muscle is made up of a flexible rubber tube braided with cross-weave sheath material and two connection flanges. When the rubber tube is inflated with compressed air, the cross-weave sheath experiences lateral expansion, resulting in axial contractive force and the change of the end point position of pneumatic muscle. Thus, the position or force control of the pneumatic muscle along its axial direction can be realized by regulating the inner pressure of its rubber tube [1]. The parallel manipulator driven by pneumatic muscles (PMDPM) studied in this paper consists of three pneumatic muscles connecting the moving platform of the parallel manipulator to its base platform, as shown in Fig. 1. By controlling the lengths of three pneumatic muscles, 3 DOF rotation motion of the parallel manipulator can be realized. Such a parallel manipulator combines the advantages of compact structure of parallel mechanisms with the adjustable stiffness and a high power/volume ratio of pneumatic muscles, which will have promising applications in robotics, industrial automation, and bionic devices [2].

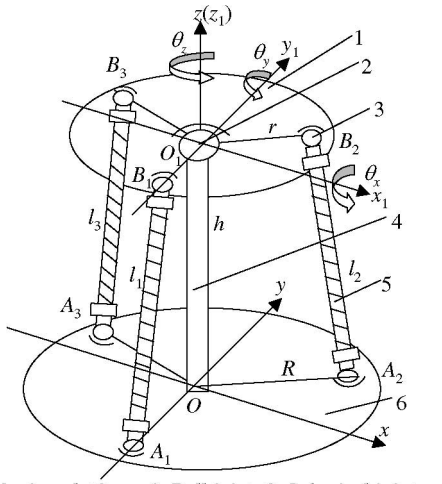

1. Moving platform 2. Ball joint 3. Spherical joint
4. Central pole 5. Pneumatic muscle 6. Base platform

Fig. 1. Structure of the PMDPM.

Due to the symmetric geometric structure of the parallel manipulator, the identical properties of the pneumatic muscles used, and no external moments around symmetry-axis direction of the parallel manipulator (i.e., z-axis in Fig. 1) acting on the moving platform, the rotation angle around z-axis is nearly close to zero during normal operations. Thus, this angle is not measured and controlled to save cost when using these types of parallel manipulators in practice, leading to a DOF redundancy in synthesizing posture controllers for the rotation angles around the other two axes. Such an added design freedom is not utilized in our previous study where an adaptive robust posture controller was developed for the PMDPM [3]. To make full use of this redundancy when the precise control of the rotation angle around z-axis is not needed, this paper will introduce an equivalent average-stiffness-like desired constraint in the adaptive

Manuscript received January 21, 2007; revised January 30, 2008. Published August 13, 2008 (projected). Recommended by Technical Editor Z. Lin. This work was supported by the National Natural Science Foundation of China (NSFC) (50775200). The work of B. Yao was supported by the NSFC under the Joint Research Fund (50528505) for Overseas Chinese Young Scholars. The material in this paper was presented in part at the 2007 American Control Conference, New York, NY, July 11–13, 2007.

X. Zhu, G. Tao, and J. Cao are with the State Key Laboratory of Fluid Power Transmission and Control, Zhejiang University, Hangzhou 310027, China (e-mail: zhuxiaoc@zju.edu.cn; gltao@zju.edu.cn; caojianjiaowang@sina.com.cn).

B. Yao is with the State Key Laboratory of Fluid Power Transmission and Control, Zhejiang University, Hangzhou 310027, China, and also with Purdue University, West Lafayette, IN 47907-2040 USA (e-mail: byao@purdue.edu).

Color versions of one or more of the figures in this paper are available online at http://ieeexplore.ieee.org.

Digital Object Identifier 10.1109/TMECH.2008.2000825

1083-4435/$25.00 © 2008 IEEE

robust posture controller design to improve posture control performance while reducing control input chattering caused by measurement noise.

The utilization of adjustable stiffness concept in the control of pneumatic muscle systems is not new and has received great attention recently. Specifically, Sui *et al.* analyzed the dynamic and static stiffness of both single pneumatic muscle and antagonistic muscle actuators [4]. Tondu and Lopez explained the natural compliant characteristics (associated with stiffness) of the actuator consisting of two pneumatic muscles set in antagonism and verified such feature by experiments on a 2 DOF selective compliant assembly robot arm (SCARA) robot prototype [5]. Liu and Zong presented the stiffness control on a manipulator driven by rubber actuators through adjusting p_0 and Δp, and furthermore, studied the compliance control of a five-bar parallel manipulator driven by rubber actuators [6], [7]. Tonietti and Bicchi employed the adaptive simultaneous position and stiffness control for a serial robot arm driven by antagonistic pneumatic muscles [8]. van der Linde [9] and Hildebrandt *et al.* [10], respectively, developed some optimization strategies on the adjustable stiffness of two opposite pneumatic muscles.

In the earlier pneumatic muscle systems with a single or antagonistic muscles, the average pressure scalar with respect to the entire stiffness of the system is adjusted to improve performance. However, especially for the PMDPM, not only it is very difficult to control the posture precisely in the presence of various parametric uncertainties and uncertain nonlinearities that are inherited to the pneumatic muscle system, but also there are added difficulties in utilizing the adjustable stiffness in the posture controller for the PMDPM with multi-input multi-output (MIMO) complex dynamics since it requires finding a uniform equivalent average stiffness scalar from the inherent multiple-dimension coupling stiffness matrix of the PMDPM.

In this paper, the adaptive robust control (ARC) strategy [11]–[13] is used to effectively deal with large extent of parametric uncertainties and uncertain nonlinearities to achieve accurate posture tracking control. In addition, with the guaranteed small tracking errors of the proposed adaptive robust posture controller, the method of adjusting the prior equivalent average stiffness is developed to eliminate the redundant DOF as well as to reduce control input chattering caused by measurement noise.

II. Principle of Posture Control With a Redundant DOF

A. Dynamics of the PMDPM With Redundancy

The PMDPM is shown in Fig. 1, which consists of a moving platform, a base platform, a central pole, and three pneumatic muscles connected by six ball joints that are evenly distributed on the respective platforms [2]. Define the posture vector as $\boldsymbol{\theta} = [\theta_x, \theta_y, \theta_z]^{\mathrm{T}}$ and the pressure vector as $\boldsymbol{p} = [p_1, p_2, p_3]^{\mathrm{T}}$, then the dynamics of the parallel manipulator is [3]

$$\begin{aligned}\boldsymbol{M}_{\mathrm{a}}(\boldsymbol{\theta})\ddot{\boldsymbol{\theta}} + \boldsymbol{C}_{\mathrm{a}}(\boldsymbol{\theta},\dot{\boldsymbol{\theta}})\dot{\boldsymbol{\theta}} + \boldsymbol{G}_{\mathrm{a}}(\boldsymbol{\theta}) \\ + \boldsymbol{F}_{\mathrm{fa}}(\boldsymbol{\theta},\dot{\boldsymbol{\theta}}) + \boldsymbol{d}_{\mathrm{ta}}(\boldsymbol{\theta},\dot{\boldsymbol{\theta}},t) = \boldsymbol{\tau}_{\mathrm{a}}\end{aligned} \tag{1}$$

where $\boldsymbol{\theta}, \dot{\boldsymbol{\theta}}, \ddot{\boldsymbol{\theta}} \in R^3$ are the posture vector, velocity vector, and acceleration vector of the parallel manipulator, respectively, $\boldsymbol{M}_{\mathrm{a}}(\boldsymbol{\theta})$ is the 3×3 rotational inertia matrix, $\boldsymbol{C}_a(\boldsymbol{\theta},\dot{\boldsymbol{\theta}})\dot{\boldsymbol{\theta}}$ is the 3-vector of centripetal and Coriolis torques [with $\boldsymbol{C}_a(\boldsymbol{\theta},\dot{\boldsymbol{\theta}})$ being a 3×3 matrix], $\boldsymbol{F}_{\mathrm{fa}}(\boldsymbol{\theta},\dot{\boldsymbol{\theta}})$ refers to all kinds of friction force torques originating from the pneumatic muscles and spherical joints, $\boldsymbol{G}_{\mathrm{a}}(\boldsymbol{\theta})$ is the 3-vector of gravitational torques, $\boldsymbol{d}_{\mathrm{ta}}(\boldsymbol{\theta},\dot{\boldsymbol{\theta}},t)$ is the disturbance vector in task space, and $\boldsymbol{\tau}_{\mathrm{a}}$ is the calculable 3-vector of torques acting on the parallel manipulator, which is given by

$$\boldsymbol{\tau}_{\mathrm{a}} = \boldsymbol{J}_{\mathrm{a}}^{\mathrm{T}}(\boldsymbol{\theta})\boldsymbol{F}_{\mathrm{m}} \tag{2}$$

where $\boldsymbol{J}_{\mathrm{a}}(\boldsymbol{\theta})$ is the Jacobian transformation matrix, $\boldsymbol{F}_{\mathrm{m}} = [F_{\mathrm{m}1}, F_{\mathrm{m}2}, F_{\mathrm{m}3}]^{\mathrm{T}}$ is the calculable contractive force vector of pneumatic muscles, and $F_{\mathrm{m}i}(i = 1, 2, 3)$ is obtained by the following integrated model that is derived from literature [14] and [15]

$$F_{\mathrm{m}i}(x_{\mathrm{m}i}, p_i) = p_i[a(1 - k_\varepsilon \varepsilon_{\mathrm{m}i})^2 - b] + F_{\mathrm{r}i}(x_{\mathrm{m}i}) \tag{3}$$

$$\begin{aligned}F_{\mathrm{r}i}(x_{\mathrm{m}i}) = -\pi D_0 L_0 \delta_0 E(1 - \varepsilon_{\mathrm{m}i})^2 \\ \times \left(\frac{1}{\sin\,\alpha_0} - \frac{1}{\sin\,\alpha_i(x_{\mathrm{m}i})}\right)\cos\,\alpha_0\end{aligned} \tag{4}$$

where $x_{\mathrm{m}i}$ is the contractive length of pneumatic muscle, p_i is the pressure inside the pneumatic muscle, a and b are constants related to the structure of pneumatic muscle, k_ε is a factor accounting for the side effect, ε_i is the contractive ratio given by $\varepsilon_i = x_{\mathrm{m}i}/L_0$, L_0 is the initial length of pneumatic muscle, $F_{\mathrm{r}i}$ is the rubber elastic force, D_0 is the initial diameter of pneumatic muscle, δ_0 is the thickness of shell and bladder, E is the bulk modulus of elasticity of the rubber tube with cross-weave sheath, α_0 is the initial braided angle of pneumatic muscle, and α_i is the current braided angle of pneumatic muscle. Note that model errors of $\boldsymbol{\tau}_{\mathrm{a}}$ from incalculable part of contractive forces are lumped into disturbances $\boldsymbol{d}_{\mathrm{ta}}$ and will be attenuated by robust feedback later.

Substituting (3) into (2), the drive moment can be described as follows:

$$\boldsymbol{\tau}_{\mathrm{a}}(\boldsymbol{\theta},\boldsymbol{p}) = \boldsymbol{f}_{\tau\mathrm{a}}(\boldsymbol{\theta})\boldsymbol{p} + \boldsymbol{g}_{\tau\mathrm{a}}(\boldsymbol{\theta}). \tag{5}$$

Two fast switching valves are used to regulate the pressure inside each pneumatic muscle, and this combination is subsequently referred to as a driving unit. And the pressure dynamics of the ith driving unit is [3], [16]

$$\dot{p}_i = -\frac{\lambda_{ai} p_i \dot{V}_i}{V_i} + \frac{\lambda_{bi} R T_i q_{\mathrm{m}i}}{V_i} + d_{\mathrm{m}i} \tag{6}$$

where λ_{ai} and λ_{bi} are different polytropic exponents, V_i is the pneumatic muscle's inner volume that is a function of $x_{\mathrm{m}i}$, R is the gas constant, T_i is the thermodynamic temperature inside the pneumatic muscle, $q_{\mathrm{m}i}$ is the calculable air mass flow rate through fast switching valve, and $d_{\mathrm{m}i}$ represents all disturbances in muscle space.

Mass flow rate $q_{\mathrm{m}i}$ is a function of the duty cycle, i.e., control input u_i given by [3]

$$q_{\mathrm{m}i}(u_i) = K_{\mathrm{q}i}(p_i, \mathrm{sign}(u_i))u_i \tag{7}$$

where $K_{\mathrm{q}i}(p_i, \mathrm{sign}(u_i))$ is a nonlinear flow gain function given by $K_{\mathrm{q}i}(p_i, \mathrm{sign}(u_i)) = A_{\mathrm{e}i}(p_{\mathrm{u}i}/\sqrt{RT_{\mathrm{u}i}})f(p_{\mathrm{d}i}/p_{\mathrm{u}i})$ with

$$f\left(\frac{p_{\mathrm{d}i}}{p_{\mathrm{u}i}}\right) = \begin{cases} \sqrt{k\left(\frac{2}{k+1}\right)^{\frac{k+1}{k-1}}}, & \text{when } 0 \le \frac{p_{\mathrm{d}i}}{p_{\mathrm{u}i}} < 0.528 \\ \sqrt{\frac{2k}{k-1}\left[\left(\frac{p_{\mathrm{d}i}}{p_{\mathrm{u}i}}\right)^{\frac{2}{k}} - \left(\frac{p_{\mathrm{d}i}}{p_{\mathrm{u}i}}\right)^{\frac{k+1}{k}}\right]}, & \text{when } 0.528 \le \frac{p_{\mathrm{d}i}}{p_{\mathrm{u}i}} \le 1 \end{cases}$$

$A_{\mathrm{e}i}$ is the effective orifice area of fast switching valve, $p_{\mathrm{u}i}$ is the upstream pressure, $p_{\mathrm{d}i}$ is the downstream pressure, $T_{\mathrm{u}i}$ is the upstream temperature, and k is the ratio of specific heat.

Due to the symmetric distribution of spherical joints, respectively, on moving platform and base platform and the identical properties of pneumatic muscles used, θ_z is nearly close to zero when no external moments around z-axis (see Fig. 1) are acting on the parallel manipulator in normal operations. Moreover, it is observed that θ_z is less than 0.2° while θ_x and θ_y normally approach 10° in simulation and experiments. For this reason, the rotation angle of z-axis is not measured and controlled in practice. Normally, θ_z is assumed to be zero in the controller design. With this assumption, the system dynamics for rotation angles around the other two axes can be written in the following form according to (1), (6), and (7):

$$\begin{cases} \boldsymbol{M}(\boldsymbol{x})\ddot{\boldsymbol{x}} + \boldsymbol{C}(\boldsymbol{x}, \dot{\boldsymbol{x}})\dot{\boldsymbol{x}} + \boldsymbol{G}(\boldsymbol{x}) \\ \qquad + \boldsymbol{F}_{\mathrm{f}}(\boldsymbol{x}, \dot{\boldsymbol{x}}) + \boldsymbol{d}_{\mathrm{t}}(\boldsymbol{x}, \dot{\boldsymbol{x}}, t) = \boldsymbol{\tau} \\ \quad = \boldsymbol{f}_{\tau}(\boldsymbol{x})\boldsymbol{p} + \boldsymbol{g}_{\tau}(\boldsymbol{x}) \\ \dot{\boldsymbol{p}} = \boldsymbol{f}_{\mathrm{m}}(\boldsymbol{x})\boldsymbol{q}_{\mathrm{m}} + \boldsymbol{g}_{\mathrm{m}}(\boldsymbol{x}, \dot{\boldsymbol{x}}, \boldsymbol{p}) + \boldsymbol{d}_{\mathrm{m}}(\boldsymbol{x}, \dot{\boldsymbol{x}}, t) \\ \boldsymbol{q}_{\mathrm{m}} = \boldsymbol{K}_{\mathrm{q}}(\boldsymbol{p}, \mathrm{sign}(\boldsymbol{u}))\boldsymbol{u} \end{cases} \tag{8}$$

where $\boldsymbol{x} = [\theta_x, \theta_y]^{\mathrm{T}} \in R^2$, $\boldsymbol{M}(\boldsymbol{x})$ and $\boldsymbol{C}(\boldsymbol{x}, \dot{\boldsymbol{x}})$ are the corresponding 2×2 components of $\boldsymbol{M}_{\mathrm{a}}(\boldsymbol{\theta})$ and $\boldsymbol{C}_{\mathrm{a}}(\boldsymbol{\theta}, \dot{\boldsymbol{\theta}})$, respectively, $\boldsymbol{G}(\boldsymbol{x})$, $\boldsymbol{F}_{\mathrm{f}}(\boldsymbol{x}, \dot{\boldsymbol{x}})$, $\boldsymbol{d}_{\mathrm{t}}(\boldsymbol{x}, \dot{\boldsymbol{x}}, t)$, $\boldsymbol{\tau}$, and $\boldsymbol{g}_{\tau}(\boldsymbol{x})$ are the corresponding 2×1 components of $\boldsymbol{G}_{\mathrm{a}}(\boldsymbol{\theta})$, $\boldsymbol{F}_{\mathrm{fa}}(\boldsymbol{\theta}, \dot{\boldsymbol{\theta}})$, $\boldsymbol{d}_{\mathrm{ta}}(\boldsymbol{\theta}, \dot{\boldsymbol{\theta}}, t)$, $\boldsymbol{\tau}_{\mathrm{a}}$, and $\boldsymbol{g}_{\tau\mathrm{a}}(\boldsymbol{\theta})$, respectively, $\boldsymbol{f}_{\tau}(\boldsymbol{x})$ is the corresponding 2×3 component of $\boldsymbol{f}_{\tau\mathrm{a}}(\boldsymbol{\theta})$, and

$$\boldsymbol{f}_{\mathrm{m}}(\boldsymbol{x}) = \mathrm{diag}\left(\left[\frac{k_{b1}RT_1}{V_1(x_{\mathrm{m}1})}, \frac{k_{b2}RT_2}{V_2(x_{\mathrm{m}2})}, \frac{k_{b3}RT_3}{V_3(x_{\mathrm{m}3})}\right]^{\mathrm{T}}\right)$$

$$\boldsymbol{g}_{\mathrm{m}}(\boldsymbol{x}, \dot{\boldsymbol{x}}, \boldsymbol{p}) = \left[-\frac{k_{a1}p_1\dot{V}_1(x_{\mathrm{m}1}, \dot{x}_{\mathrm{m}1})}{V_1(x_{\mathrm{m}1})}, -\frac{k_{a2}p_2\dot{V}_2(x_{\mathrm{m}2}, \dot{x}_{\mathrm{m}2})}{V_2(x_{\mathrm{m}2})}, -\frac{k_{a3}p_3\dot{V}_3(x_{\mathrm{m}3}, \dot{x}_{\mathrm{m}3})}{V_3(x_{\mathrm{m}3})}\right]^{\mathrm{T}}.$$

B. Utilization of Equivalent Average Stiffness

Since the rotation around z-axis is not controlled in normal operations for the PMDPM, there exists a DOF redundancy in synthesizing the posture controller for rotation angles around the other two axes. Therefore, an equivalent average-stiffness-like constraint, which is related to the multiple-dimension equivalent stiffness matrix of the PMDPM, is introduced into the posture controller for removing such a DOF redundancy.

With the backstepping design procedure, the desired drive moment $\boldsymbol{\tau}_{\mathrm{d}}$ in the task space can be calculated by desired and actual postures under certain control strategy. And then, according to the first equation of (8), the desired pressure vector $\boldsymbol{p}_{\mathrm{d}}$ can be derived from the following equation:

$$\boldsymbol{\tau}_{\mathrm{d}}(\boldsymbol{x}, \dot{\boldsymbol{x}}, \boldsymbol{x}_{\mathrm{d}}, \dot{\boldsymbol{x}}_{\mathrm{d}}, \ddot{\boldsymbol{x}}_{\mathrm{d}}) = \boldsymbol{f}_{\tau}(\boldsymbol{x})\boldsymbol{p}_{\mathrm{d}} + \boldsymbol{g}_{\tau}(\boldsymbol{x}). \tag{9}$$

However, the solution of $\boldsymbol{p}_{\mathrm{d}}$ from $\boldsymbol{\tau}_{\mathrm{d}}$ along (9) is not unique since $\boldsymbol{f}_{\tau}(\boldsymbol{x})$ is a 2×3 matrix while $\boldsymbol{p}_{\mathrm{d}}$ is a 3×1 vector and $\boldsymbol{\tau}_{\mathrm{d}}$ is a 2×1 vector. That is, the system possesses a DOF redundancy. Therefore, an extra constraint related to the pressure vector $\boldsymbol{p}$ is introduced into the posture controller for removing the redundancy.

Under the condition of the parallel manipulator being at the equilibrium state ($\boldsymbol{x} = \dot{\boldsymbol{x}} = \ddot{\boldsymbol{x}} = [0^\circ, 0^\circ]^{\mathrm{T}}$) and $\partial\boldsymbol{p}/\partial\boldsymbol{\theta} \approx 0$, an equivalent stiffness is described as (10) according to (5), which is the posture derivative of the drive moment [6], [17]

$$\boldsymbol{K}(\boldsymbol{p}, \boldsymbol{\theta}_{\mathrm{a}}) = \frac{\partial \boldsymbol{f}_{\tau\mathrm{a}}}{\partial \boldsymbol{\theta}_{\mathrm{a}}}\boldsymbol{p} + \frac{\partial \boldsymbol{g}_{\tau\mathrm{a}}}{\partial \boldsymbol{\theta}_{\mathrm{a}}}. \tag{10}$$

It can be seen from this equation that the equivalent stiffness is mainly dependent on the inner pressures of pneumatic muscles and the posture vector of the PMDPM. Due to the symmetric distribution of spherical joints on moving platform and base platform as well as the identical properties of pneumatic muscles, the equivalent stiffness is a principle diagonal matrix, whose components have the feature that magnitudes of the equivalent stiffness around x- and y-axes are at the same level and larger than that around z-axis.

Then, an equivalent average stiffness of the parallel manipulator is defined as $K_{\mathrm{d}} = (K_x + K_y)/2$ and expressed as the following equation, which is also dependent on inner pressures of three pneumatic muscles:

$$K_{\mathrm{d}} = \boldsymbol{f}_{\mathrm{k}}(\boldsymbol{x})\boldsymbol{p} + g_{\mathrm{k}}(\boldsymbol{x}). \tag{11}$$

Therefore, integrating with (9) and (11), the desired pressure vector in the task space is uniquely determined by

$$\boldsymbol{p}_{\mathrm{d}} = \boldsymbol{\psi}_1^{-1}(\boldsymbol{x})[\boldsymbol{\upsilon} - \boldsymbol{\psi}_2(\boldsymbol{x})] \tag{12}$$

where

$$\boldsymbol{\psi}_1(\boldsymbol{x}) = \begin{bmatrix} \boldsymbol{f}_{\tau}(\boldsymbol{x}) \\ \boldsymbol{f}_{\mathrm{k}}(\boldsymbol{x}) \end{bmatrix}, \quad \boldsymbol{\psi}_2(\boldsymbol{x}) = \begin{bmatrix} \boldsymbol{g}_{\tau}(\boldsymbol{x}) \\ g_{\mathrm{k}}(\boldsymbol{x}) \end{bmatrix}, \quad \boldsymbol{\upsilon} = \begin{bmatrix} \boldsymbol{\tau}_{\mathrm{d}} \\ K_{\mathrm{d}} \end{bmatrix}.$$

In the following design, for notation simplicity, the variable $\boldsymbol{M}(\boldsymbol{x})$ is expressed by $\boldsymbol{M}$, and other variables are analogical when no confusions on the function variables are concerned.

III. Controller Design

A. Schematic Diagram of the Posture Controller

The posture controller for the PMDPM is composed of two parts: the ARC design and the equivalent average stiffness design. The ARC is adopted to deal with rather severe parametric uncertainties and uncertain nonlinearities existing in the dynamics of the PMDPM [3], [11], [13], both due to the time-varying friction forces and the static force modeling errors of pneumatic

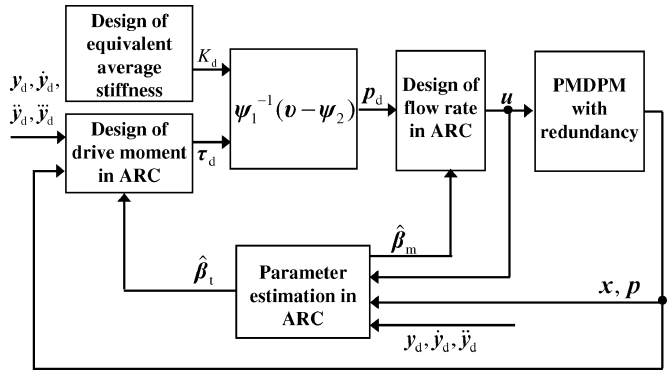

Fig. 2. Schematic diagram of the posture controller.

muscles and due to the inherent complex nonlinearities and unknown disturbances of the parallel manipulator. Meanwhile, the equivalent average stiffness is employed to make full use of the redundancy of the PMDPM for reducing control input chattering caused by measurement noise. It is noted that since there exist unmatched model uncertainties in the dynamics of the PMDPM, the backstepping design is adopted consisting of desired drive moment design and desired flow rate design along with parameter adaptation to compensate for large parametric uncertainties. The schematic diagram of the adaptive robust posture controller with adjustable equivalent average stiffness is shown in Fig. 2.

B. Assumption and Projection Mapping

In general, the system is subjected to parametric uncertainties due to unknown values of λ_a, λ_b, the unknown parameters in $\boldsymbol{M}(\boldsymbol{x})$, $\boldsymbol{C}(\boldsymbol{x},\dot{\boldsymbol{x}})$, $\boldsymbol{G}(\boldsymbol{x})$, $\boldsymbol{F}_{\rm f}(\boldsymbol{x},\dot{\boldsymbol{x}})$, and the unknown nominal value of the lumped disturbance vector represented by $\boldsymbol{d}_{\rm t0}$ and $\boldsymbol{d}_{\rm m0}$. Thus, let $\boldsymbol{\beta}$ be the unknown parameter vector whose components are the aforementioned unknown parameters. In addition, there exist uncertain nonlinearities represented by $\boldsymbol{d}_{\rm t}$ and $\boldsymbol{d}_{\rm m}$ in the system ($\boldsymbol{d}_{\rm t}=\boldsymbol{d}_{\rm t0}+\tilde{\boldsymbol{d}}_{\rm t}$, $\boldsymbol{d}_{\rm m}=\boldsymbol{d}_{\rm m0}+\tilde{\boldsymbol{d}}_{\rm m}$). Assume that the extents of the parametric uncertainties and uncertain nonlinearities are known as

$$\begin{aligned}\boldsymbol{\beta}\in\Omega_\beta=\{\boldsymbol{\beta}:\boldsymbol{\beta}_{\min}\le\boldsymbol{\beta}\le\boldsymbol{\beta}_{\max}\}\\ |\tilde{\boldsymbol{d}}_{\rm t}|\le\boldsymbol{d}_{\rm tmax},\quad |\tilde{\boldsymbol{d}}_{\rm m}|\le\boldsymbol{d}_{\rm mmax}\end{aligned}\tag{13}$$

where $\boldsymbol{\beta}_{\max}=[\beta_{1\max},\ldots,\beta_{n\max}]^{\rm T}$ is the maximum parameter vector, $\boldsymbol{\beta}_{\min}=[\beta_{1\min},\ldots,\beta_{n\min}]^{\rm T}$ is the minimum parameter vector, and $\boldsymbol{d}_{\rm tmax}$ and $\boldsymbol{d}_{\rm mmax}$ are known vectors.

Let $\hat{\boldsymbol{\beta}}$ denote the estimate of $\boldsymbol{\beta}$ and $\tilde{\boldsymbol{\beta}}=\hat{\boldsymbol{\beta}}-\boldsymbol{\beta}$ the estimation error. In view of (13), a discontinuous projection can be defined as (14) in order to guarantee that the parameter estimates given by (15) remain in the known bounded region all the time [11], [13]:

$$\mathrm{Proj}_{\hat{\boldsymbol{\beta}}}(\bullet_i)=\begin{cases}0, & \text{if } \hat{\beta}_i=\beta_{i\max} \text{ and } \bullet_i>0\\ 0, & \text{if } \hat{\beta}_i=\beta_{i\min} \text{ and } \bullet_i<0\\ \bullet_i, & \text{otherwise}.\end{cases}\tag{14}$$

The adaptation law is given by

$$\dot{\hat{\boldsymbol{\beta}}}=\mathrm{Proj}_{\hat{\boldsymbol{\beta}}}(\boldsymbol{\Gamma}\boldsymbol{\sigma}),\qquad \hat{\boldsymbol{\beta}}(0)\in\Omega_\beta\tag{15}$$

where $\boldsymbol{\Gamma}>0$ is a diagonal matrix and $\boldsymbol{\sigma}$ is a parameter adaptation function to be synthesized later. It can be shown that for any adaptation function, the projection mapping used in (15) guarantees

$$\begin{cases}\hat{\boldsymbol{\beta}}\in\Omega_\beta=\{\hat{\boldsymbol{\beta}}:\boldsymbol{\beta}_{\min}\le\hat{\boldsymbol{\beta}}\le\boldsymbol{\beta}_{\max}\}\\ \tilde{\boldsymbol{\beta}}^{\rm T}[\boldsymbol{\Gamma}^{-1}\mathrm{Proj}_{\hat{\boldsymbol{\beta}}}(\boldsymbol{\Gamma}\boldsymbol{\sigma})-\boldsymbol{\sigma}]\le 0\qquad\forall\boldsymbol{\sigma}.\end{cases}\tag{16}$$

C. Design of ARC

In this section, the ARC will be synthesized using the recursive backstepping procedure for the system (8) to achieve a guaranteed transient and final tracking accuracy [3], [11], [13].

1) Design of Desired Drive Moment: Define a switching-function-like quantity as

$$\boldsymbol{z}_2=\dot{\boldsymbol{z}}_1+\boldsymbol{K}_{\rm c}\boldsymbol{z}_1\tag{17}$$

where $\boldsymbol{z}_1=\boldsymbol{x}-\boldsymbol{y}_{\rm d}$ is the trajectory tracking error vector and $\boldsymbol{K}_{\rm c}$ is a positive diagonal feedback matrix. If $\boldsymbol{z}_2$ converges to a small value or zero, then $\boldsymbol{z}_1$ will converge to a small value or zero since the transfer function from $\boldsymbol{z}_2$ to $\boldsymbol{z}_1$ $G(s)=\boldsymbol{I}(s+\boldsymbol{K}_{\rm c})^{-1}$ is globally asymptotically stable. Thereby, the next objective is to design the drive moment $\boldsymbol{\tau}$ for making $\boldsymbol{z}_2$ as small as possible.

Defining $\dot{\boldsymbol{x}}_{\rm r}=\dot{\boldsymbol{y}}_{\rm d}-\boldsymbol{K}_{\rm c}\boldsymbol{z}_1$, the terms including parametric uncertainties in the task space can be described as (18) with a set of unknown parameter vector $\boldsymbol{\beta}_{\rm t}$ in the task space:

$$\begin{aligned}&\boldsymbol{M}\ddot{\boldsymbol{x}}_{\rm r}+\boldsymbol{C}\dot{\boldsymbol{x}}_{\rm r}+\boldsymbol{F}_{\rm f}+\boldsymbol{G}+\boldsymbol{d}_{\rm t0}\\ &\quad=\boldsymbol{\varphi}_2^{\rm T}(\boldsymbol{x},\dot{\boldsymbol{x}},\dot{\boldsymbol{x}}_{\rm r},\ddot{\boldsymbol{x}}_{\rm r})\boldsymbol{\beta}_{\rm t}+\boldsymbol{f}_{\rm c2}(\boldsymbol{x},\dot{\boldsymbol{x}},\dot{\boldsymbol{x}}_{\rm r},\ddot{\boldsymbol{x}}_{\rm r})\end{aligned}\tag{18}$$

where $\boldsymbol{\varphi}_2^{\rm T}(\boldsymbol{x},\dot{\boldsymbol{x}},\dot{\boldsymbol{x}}_{\rm r},\ddot{\boldsymbol{x}}_{\rm r})$ is the corresponding regressor of $\boldsymbol{\beta}_{\rm t}$ and $\boldsymbol{f}_{\rm c2}(\boldsymbol{x},\dot{\boldsymbol{x}},\dot{\boldsymbol{x}}_{\rm r},\ddot{\boldsymbol{x}}_{\rm r})$ is the known nonlinear term.

The following equation could be obtained along the solution of (8) and (18):

$$\boldsymbol{M}\dot{\boldsymbol{z}}_2+\boldsymbol{C}\boldsymbol{z}_2=\boldsymbol{\tau}-\boldsymbol{\varphi}_2^{\rm T}\hat{\boldsymbol{\beta}}_{\rm t}-\boldsymbol{f}_{\rm c2}+\boldsymbol{\varphi}_2^{\rm T}\tilde{\boldsymbol{\beta}}_{\rm t}-\tilde{\boldsymbol{d}}_{\rm t}.\tag{19}$$

The desired drive moment $\boldsymbol{\tau}_{\rm d}$ is given by

$$\boldsymbol{\tau}_{\rm d}=\boldsymbol{\tau}_{\rm da}+\boldsymbol{\tau}_{\rm ds},\qquad \boldsymbol{\tau}_{\rm da}=\boldsymbol{\varphi}_2^{\rm T}\hat{\boldsymbol{\beta}}_{\rm t}+\boldsymbol{f}_{\rm c2}\tag{20}$$

where $\boldsymbol{\tau}_{\rm da}$ functions as the adaptive control part used to achieve an improved model compensation through online parameter adaptation via $\hat{\boldsymbol{\beta}}_{\rm t}$, and $\boldsymbol{\tau}_{\rm ds}$ is a robust control law to be synthesized later. $\hat{\boldsymbol{\beta}}_{\rm t}$ is updated by a discontinuous projection-based adaptation law of the form (15), i.e., $\dot{\hat{\boldsymbol{\beta}}}_{\rm t}=\mathrm{Proj}_{\hat{\beta}}(\boldsymbol{\Gamma}_2\boldsymbol{\sigma}_2)$ with the parameter adaptation function $\boldsymbol{\sigma}_2=-\boldsymbol{\varphi}_2\boldsymbol{z}_2$. $\boldsymbol{\tau}_{\rm ds}$ consists of two parts

$$\boldsymbol{\tau}_{\rm ds}=\boldsymbol{\tau}_{\rm ds1}+\boldsymbol{\tau}_{\rm ds2},\qquad \boldsymbol{\tau}_{\rm ds1}=-\boldsymbol{K}_2\boldsymbol{z}_2\tag{21}$$

where $\boldsymbol{K}_2$ is a positive definite feedback gain matrix and $\boldsymbol{\tau}_{\rm ds2}$ is synthesized to dominate the uncompensated model uncertainties

coming from both parametric uncertainties and uncertain nonlinearities, which is chosen to satisfy the following conditions:

$$\begin{cases} \boldsymbol{z}_2^{\mathrm{T}}(\boldsymbol{\tau}_{\mathrm{ds2}} + \boldsymbol{\varphi}_2^{\mathrm{T}}\tilde{\boldsymbol{\beta}}_{\mathrm{t}} - \tilde{\boldsymbol{d}}_{\mathrm{t}}) \le \boldsymbol{\varepsilon}_2 \\ \boldsymbol{z}_2^{\mathrm{T}}\boldsymbol{\tau}_{\mathrm{ds2}} \le 0 \end{cases} \tag{22}$$

where ε_2 is a positive design parameter. For example, $\boldsymbol{\tau}_{\mathrm{ds2}}$ may be chosen as [13]

$$\boldsymbol{\tau}_{\mathrm{ds2}} = -\boldsymbol{K}_{2\mathrm{s}} \tanh(\boldsymbol{z}_2/\varepsilon_2) \tag{23}$$

where $\boldsymbol{K}_{2\mathrm{s}}$ is a positive definite diagonal matrix dependent on uncertain nonlinearities in the task space.

As analyzed in Section II, according to the desired drive moment $\boldsymbol{\tau}_{\mathrm{d}}$ and the desired equivalent average stiffness K_{d} designed later, the desired pressure vector $\boldsymbol{p}_{\mathrm{d}}$ can be obtained from (12).

Define the positive semidefinite Lyapunov function $V_2 = (1/2)\boldsymbol{z}_2^{\mathrm{T}}\boldsymbol{M}\boldsymbol{z}_2$ and let the input discrepancy be $\boldsymbol{z}_3 = \boldsymbol{p} - \boldsymbol{p}_{\mathrm{d}}$. The time derivative of V_2 along the solution of (19) is

$$\begin{aligned} \dot{V}_2 =& -\boldsymbol{z}_2^{\mathrm{T}}\boldsymbol{K}_2\boldsymbol{z}_2 + \boldsymbol{z}_2^{\mathrm{T}}\boldsymbol{f}_{\tau}\boldsymbol{z}_3 \\ &+ \boldsymbol{z}_2^{\mathrm{T}}(\boldsymbol{\tau}_{\mathrm{ds2}} + \boldsymbol{\varphi}_2^{\mathrm{T}}\tilde{\boldsymbol{\beta}}_{\mathrm{t}} - \tilde{\boldsymbol{d}}_{\mathrm{t}}). \end{aligned} \tag{24}$$

2) Design of Desired Flow Rate: Next, the mass flow rate $\boldsymbol{q}_{\mathrm{m}}$ is synthesized so that $\boldsymbol{z}_3$ converges to a small value or zero with a guaranteed transient performance. With a set of unknown parameter vector $\boldsymbol{\beta}_{\mathrm{m}}$ in muscle space, the terms including parametric uncertainties in muscle space are described as

$$\begin{aligned} &\boldsymbol{f}_{\mathrm{m}}(\boldsymbol{x})\boldsymbol{q}_{\mathrm{m}} + \boldsymbol{g}_{\mathrm{m}}(\boldsymbol{x}, \dot{\boldsymbol{x}}, \boldsymbol{p}) + \boldsymbol{d}_{\mathrm{m0}} \\ &\quad = \boldsymbol{\varphi}_3^{\mathrm{T}}(\boldsymbol{x}, \dot{\boldsymbol{x}}, \boldsymbol{p})\boldsymbol{\beta}_{\mathrm{m}} + \boldsymbol{f}_{\mathrm{c3}}(\boldsymbol{x}, \dot{\boldsymbol{x}}, \boldsymbol{p}) \end{aligned} \tag{25}$$

where $\boldsymbol{\varphi}_3^{\mathrm{T}}(\boldsymbol{x}, \dot{\boldsymbol{x}}, \boldsymbol{p})$ is the corresponding regressor of $\boldsymbol{\beta}_{\mathrm{m}}$ and $\boldsymbol{f}_{\mathrm{c3}}(\boldsymbol{x}, \dot{\boldsymbol{x}}, \boldsymbol{p})$ is the known nonlinear term.

The time derivative of the input discrepancy along the solution of (8) and (12) is

$$\begin{aligned} \dot{\boldsymbol{z}}_3 =& \dot{\boldsymbol{p}} - \dot{\boldsymbol{p}}_{\mathrm{d}} = \boldsymbol{f}_{\mathrm{m}}\boldsymbol{q}_{\mathrm{m}} + \boldsymbol{g}_{\mathrm{m}} + \boldsymbol{d}_{\mathrm{m0}} \\ &+ \tilde{\boldsymbol{d}}_{\mathrm{m}} - \dot{\boldsymbol{p}}_{\mathrm{dc}} - \dot{\boldsymbol{p}}_{\mathrm{du}} \end{aligned} \tag{26}$$

where $\dot{\boldsymbol{p}}_{\mathrm{dc}} = \partial\boldsymbol{p}_{\mathrm{d}}/\partial t + (\partial\boldsymbol{p}_{\mathrm{d}}/\partial\boldsymbol{x})\hat{\dot{\boldsymbol{x}}} + (\partial\boldsymbol{p}_{\mathrm{d}}/\partial\dot{\boldsymbol{x}})\hat{\ddot{\boldsymbol{x}}} + (\partial\boldsymbol{p}_{\mathrm{d}}/\partial\hat{\boldsymbol{\beta}}_{\mathrm{t}})\dot{\hat{\boldsymbol{\beta}}}_{\mathrm{t}}$ and $\dot{\boldsymbol{p}}_{\mathrm{du}} = (\partial\boldsymbol{p}_{\mathrm{d}}/\partial\boldsymbol{x})(\dot{\boldsymbol{x}} - \hat{\dot{\boldsymbol{x}}}) + (\partial\boldsymbol{p}_{\mathrm{d}}/\partial\dot{\boldsymbol{x}})(\ddot{\boldsymbol{x}} - \hat{\ddot{\boldsymbol{x}}})$ in which $\hat{\dot{\boldsymbol{x}}}$ and $\hat{\ddot{\boldsymbol{x}}}$ are obtained from $\boldsymbol{x}$ by a second-order differential filter as [3], $\dot{\boldsymbol{p}}_{\mathrm{dc}}$ represents the calculable part of $\dot{\boldsymbol{p}}_{\mathrm{d}}$ and can be used to design control input $\boldsymbol{u}$, but $\dot{\boldsymbol{p}}_{\mathrm{du}}$ cannot due to various uncertainties.

The desired mass flow rate $\boldsymbol{q}_{\mathrm{md}}$ is

$$\begin{aligned} \boldsymbol{q}_{\mathrm{md}} &= \boldsymbol{q}_{\mathrm{mda}} + \boldsymbol{q}_{\mathrm{mds}}, \\ \boldsymbol{q}_{\mathrm{mda}} &= \hat{\boldsymbol{f}}_{\mathrm{m}}^{-1}(-\boldsymbol{f}_{\tau}^{\mathrm{T}}\boldsymbol{z}_2 - \hat{\boldsymbol{g}}_{\mathrm{m}} - \hat{\boldsymbol{d}}_{\mathrm{m0}} + \dot{\boldsymbol{p}}_{\mathrm{dc}}) \end{aligned} \tag{27}$$

where $\boldsymbol{q}_{\mathrm{mda}}$ is used for adaptive model compensation through online parameter adaptation via $\hat{\boldsymbol{\beta}}_{\mathrm{m}}$, and $\boldsymbol{q}_{\mathrm{mds}}$ is the robust control law to be synthesized later. $\hat{\boldsymbol{\beta}}_{\mathrm{m}}$ is updated by a discontinuous projection-based adaptation law of the form (15), i.e., $\dot{\hat{\boldsymbol{\beta}}}_{\mathrm{m}} = \mathrm{Proj}_{\hat{\boldsymbol{\beta}}}(\boldsymbol{\Gamma}_3\boldsymbol{\sigma}_3)$ with the parameter adaptation function $\boldsymbol{\sigma}_3 = \boldsymbol{\varphi}_3\boldsymbol{z}_3$.

The robust control law $\boldsymbol{q}_{\mathrm{mds}}$ consists of the following two parts:

$$\boldsymbol{q}_{\mathrm{mds}} = \boldsymbol{q}_{\mathrm{mds1}} + \boldsymbol{q}_{\mathrm{mds2}}, \qquad \boldsymbol{q}_{\mathrm{mds1}} = -\hat{\boldsymbol{f}}_{\mathrm{m}}^{-1}\boldsymbol{K}_3\boldsymbol{z}_3 \tag{28}$$

where $\boldsymbol{K}_3$ is a positive definite feedback gain matrix and $\boldsymbol{q}_{\mathrm{mds2}}$ is synthesized to dominate the uncompensated model uncertainties and chosen to satisfy the following conditions:

$$\begin{cases} \boldsymbol{z}_3^{\mathrm{T}}(\hat{\boldsymbol{f}}_{\mathrm{m}}\boldsymbol{q}_{\mathrm{mds2}} - \boldsymbol{\varphi}_3^{\mathrm{T}}\tilde{\boldsymbol{\beta}}_{\mathrm{m}} + \tilde{\boldsymbol{d}}_{\mathrm{m}} - \dot{\boldsymbol{p}}_{\mathrm{du}}) \le \varepsilon_3 \\ \boldsymbol{z}_3^{\mathrm{T}}\hat{\boldsymbol{f}}_{\mathrm{m}}\boldsymbol{q}_{\mathrm{mds2}} \le 0 \end{cases} \tag{29}$$

where ε_3 is a positive design parameter that may be arbitrarily small. For example, $\boldsymbol{q}_{\mathrm{mds2}}$ may be chosen as [13]

$$\boldsymbol{q}_{\mathrm{mds2}} = -\hat{\boldsymbol{f}}_{\mathrm{m}}^{-1}\boldsymbol{K}_{3\mathrm{s}} \tanh(\boldsymbol{z}_3/\varepsilon_3) \tag{30}$$

where $\boldsymbol{K}_{3\mathrm{s}}$ is a positive definite diagonal matrix dependent on uncertain nonlinearities in muscle space.

To see how this control function works, define a positive semidefinite (p.s.d.) function $V_3 = V_2 + (1/2)\boldsymbol{z}_3^{\mathrm{T}}\boldsymbol{z}_3$, its time derivative along the solution of (22), (24), (26), and (29) is

$$\dot{V}_3 \le -\boldsymbol{z}_2^{\mathrm{T}}\boldsymbol{K}_1\boldsymbol{z}_2 - \boldsymbol{z}_3^{\mathrm{T}}\boldsymbol{K}_3\boldsymbol{z}_3 + \varepsilon_2 + \varepsilon_3. \tag{31}$$

According to comparison lemma [18], the solution of (31) is

$$V_3(t) \le \exp(-\lambda_v t)V_3(0) + \frac{\varepsilon_v}{\lambda_v}[1 - \exp(-\lambda_v t)] \tag{32}$$

where $\lambda_v = 2 \times \min\{\boldsymbol{K}_2, \boldsymbol{K}_3\}$ and $\varepsilon_v = \varepsilon_2 + \varepsilon_3$.

As can be seen from (32), the output tracking error vector $\boldsymbol{z} = [\boldsymbol{z}_2^{\mathrm{T}}, \boldsymbol{z}_3^{\mathrm{T}}]^{\mathrm{T}}$ is bounded above by

$$\begin{aligned} \|\boldsymbol{z}(t)\|^2 <& \exp(-\lambda_v t)\,\|\boldsymbol{z}(0)\| \\ &+ \frac{2\varepsilon_v}{\lambda_v}[1 - \exp(-\lambda_v t)]. \end{aligned} \tag{33}$$

Specifically, asymptotic output tracking (or zero final tracking error) is obtained in the presence of parametric uncertainties only.

3) Design of Control Input Vector: Once the desired mass flow rate $\boldsymbol{q}_{\mathrm{md}}$ is synthesized, the inverse flow rate mapping is used to calculate the specific duty cycle commands of fast switching valves. The control input vector is

$$\boldsymbol{u} = \boldsymbol{K}_{\mathrm{q}}^{-1}\boldsymbol{q}_{\mathrm{md}}. \tag{34}$$

D. Design of Equivalent Average Stiffness

The equivalent average stiffness K_{d} in (12) is adjustable and can be further designed to reduce control input chattering.

1) Permissible Equivalent Average Stiffness: The equivalent average stiffness K_{d} is constrained by the minimum and maximum permissible inner pressures of three pneumatic muscles.

For this purpose, (3) can be written in another form as

$$F_{\mathrm{m}i}(x_{\mathrm{m}i}, p_i) = A_i(x_{\mathrm{m}i})p_i + F_{\mathrm{r}i}(x_{\mathrm{m}i}) \tag{35}$$

where $A_i(x_{\mathrm{m}i})$ is the equivalent acting area of the pneumatic muscle.

For a single pneumatic muscle, the minimum inner pressure is $p_{\mathrm{min}i} = -F_{\mathrm{r}i}(x_{\mathrm{m}i})/A_i(x_{\mathrm{m}i})$ since pneumatic muscle can only generate positive contractive force. Meanwhile, the maximum inner pressure is $p_{\mathrm{max}i} = \min(p_{\mathrm{m}i}, p_{\mathrm{s}})$ in which $p_{\mathrm{m}i}$ is the permissible maximum inner pressure of the pneumatic muscle and p_{s} is the supply pressure. Let $\boldsymbol{p}_{\mathrm{min}}$ be the vector consisting of such three $\boldsymbol{p}_{\mathrm{min}i}$ and $\boldsymbol{p}_{\mathrm{max}}$ be the vector consisting of such three $p_{\mathrm{max}i}$.

According to (12), the permissible desired pressure vector should satisfy the following inequality:

$$\boldsymbol{p}_{\mathrm{min}} \le \boldsymbol{p}_{\mathrm{d}} = \boldsymbol{\psi}_1^{-1}(\boldsymbol{\upsilon} - \boldsymbol{\psi}_2) \le \boldsymbol{p}_{\mathrm{max}}. \tag{36}$$

Let $\boldsymbol{\psi}_1^{-1}\boldsymbol{\upsilon} = \boldsymbol{a}_\tau \boldsymbol{\tau}_{\mathrm{d}} + \boldsymbol{a}_k K_{\mathrm{d}}$ in which $\boldsymbol{a}_\tau$ is a 3×2 matrix and a_k is a 3×1 matrix from $\boldsymbol{\psi}_1^{-1}$, and substitute it into (36), then

$$\boldsymbol{p}_{\mathrm{min}} + \boldsymbol{\psi}_1^{-1}\boldsymbol{\psi}_2 - \boldsymbol{a}_\tau \boldsymbol{\tau}_{\mathrm{d}} \le \boldsymbol{a}_k K_{\mathrm{d}} \le \boldsymbol{p}_{\mathrm{max}} + \boldsymbol{\psi}_1^{-1}\boldsymbol{\psi}_2 - \boldsymbol{a}_\tau \boldsymbol{\tau}_{\mathrm{d}}. \tag{37}$$

Hence, the permissible equivalent average stiffness for the desired posture is obtained:

$$\begin{aligned} K_{\mathrm{dmax}} &= \min\left\{\left(\frac{\chi_{r1}}{a_{k1}}\right), \left(\frac{\chi_{r2}}{a_{k2}}\right), \left(\frac{\chi_{r3}}{a_{k3}}\right)\right\} \\ K_{\mathrm{dmin}} &= \max\left\{\left(\frac{\chi_{l1}}{a_{k1}}\right), \left(\frac{\chi_{l2}}{a_{k2}}\right), \left(\frac{\chi_{l3}}{a_{k3}}\right)\right\} \end{aligned} \tag{38}$$

where $\boldsymbol{\chi}_r = \boldsymbol{p}_{\mathrm{max}} + \boldsymbol{\psi}_1^{-1}\boldsymbol{\psi}_2 - \boldsymbol{a}_\tau \boldsymbol{\tau}_{\mathrm{d}} = [\chi_{r1}, \chi_{r2}, \chi_{r3}]^{\mathrm{T}}$ and $\boldsymbol{\chi}_l = \boldsymbol{p}_{\mathrm{min}} + \boldsymbol{\psi}_1^{-1}\boldsymbol{\psi}_2 - \boldsymbol{a}_\tau \boldsymbol{\tau}_{\mathrm{d}} = [\chi_{l1}, \chi_{l2}, \chi_{l3}]^{\mathrm{T}}$.

2) Optimal Equivalent Average Stiffness: Generally, the equivalent average stiffness of the PMDPM has arbitrariness within the permissible range when not controlled, which indicates that it may be used as a constraint to tune system performance. Concretely, the velocity and acceleration of the PMDPM would be needed in the calculation of the control input vector. Though these signals may be obtained from the posture through a second-order differential filter, measurement noise may be amplified resulting in severe control input chattering. Thus, it is necessary to find an optimal equivalent average stiffness for decreasing the gain from noise to control input vector, and consequently, reducing control input chattering.

The acceleration in control input vector consists of the following two parts:

$$\hat{\ddot{\boldsymbol{x}}} = \hat{\ddot{\boldsymbol{x}}}_0 + \boldsymbol{n}(t) \tag{39}$$

where $\hat{\ddot{\boldsymbol{x}}}_0$ is the noise-free signal and $\boldsymbol{n}(t)$ is the measurement noise. When the trajectory tracking error is small, $\boldsymbol{p}_{\mathrm{d}}$ is nearly equal to $\boldsymbol{p}$ and the robust control part is neglected. With this approximation, the control input vector in (34) can be rewritten as

$$\boldsymbol{u} = \boldsymbol{K}_{\mathrm{q}}^{-1}(\boldsymbol{p}_{\mathrm{d}}(K_{\mathrm{d}}))\hat{\boldsymbol{f}}_{\mathrm{m}}^{-1}\frac{\partial \boldsymbol{p}_{\mathrm{d}}(K_{\mathrm{d}})}{\partial \dot{\boldsymbol{x}}}\left[\hat{\ddot{\boldsymbol{x}}}_0 + \boldsymbol{n}(t)\right] + \boldsymbol{\kappa}(\boldsymbol{x}, \hat{\dot{\boldsymbol{x}}}, t) \tag{40}$$

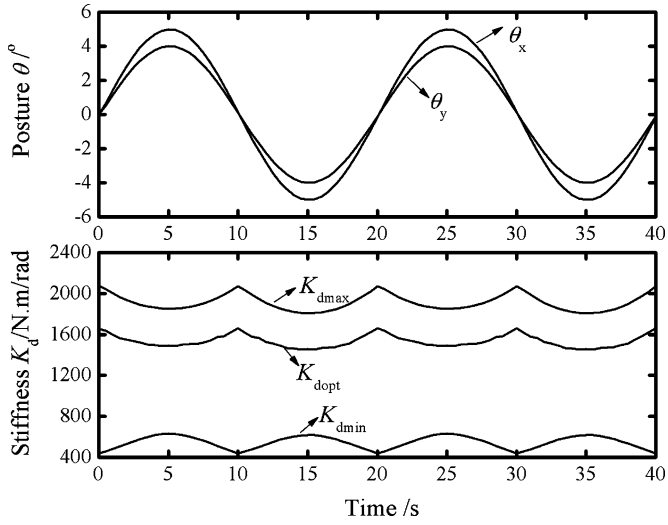

Fig. 3. Permissible and optimal equivalent average stiffness along a sinusoidal trajectory.

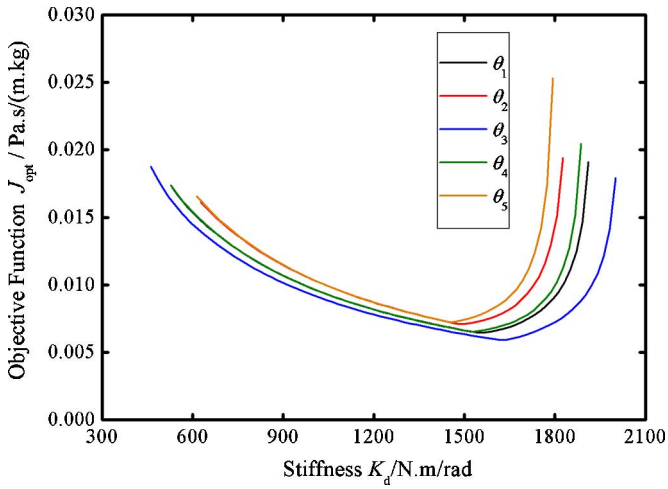

Fig. 4. Relation between J_{opt} and K_{d} at different posture points in the process of tracking the trajectory. *Note:* $\boldsymbol{\theta}_1$, $\boldsymbol{\theta}_2$, $\boldsymbol{\theta}_3$, $\boldsymbol{\theta}_4$, and $\boldsymbol{\theta}_5$ represent different posture points. $\boldsymbol{\theta}_1 = [2.8229°, 2.2583°]^{\mathrm{T}}$, $\boldsymbol{\theta}_2 = [4.9134°, 3.9308°]^{\mathrm{T}}$, $\boldsymbol{\theta}_3 = [0.9213°, 0.7370°]^{\mathrm{T}}$, $\boldsymbol{\theta}_4 = [-2.8229°, -2.2583°]^{\mathrm{T}}$, and $\boldsymbol{\theta}_5 = [-4.9134°, -3.9308°]^{\mathrm{T}}$.

where $\boldsymbol{\kappa}(\boldsymbol{x}, \hat{\dot{\boldsymbol{x}}}, t)$ is a nonlinear function given by

$$\boldsymbol{\kappa}(\boldsymbol{x}, \hat{\dot{\boldsymbol{x}}}, t) = \boldsymbol{K}_{\mathrm{q}}^{-1}\hat{\boldsymbol{f}}_{\mathrm{m}}^{-1}\left[\frac{\partial \boldsymbol{p}_{\mathrm{d}}}{\partial t} + \frac{\partial \boldsymbol{p}_{\mathrm{d}}}{\partial \boldsymbol{x}}\hat{\dot{\boldsymbol{x}}} + \frac{\partial \boldsymbol{p}_{\mathrm{d}}}{\partial \hat{\boldsymbol{\beta}}_{\mathrm{t}}}\dot{\hat{\boldsymbol{\beta}}}_{\mathrm{t}} - \hat{\boldsymbol{g}}_{\mathrm{m}} - \hat{\boldsymbol{d}}_{\mathrm{m}0}\right].$$

In order to obtain the optimal equivalent average stiffness, the gain from noise to control input vector should be as small as possible. Thus, the objective function to be minimized is

$$J_{\mathrm{opt}} = \left|\boldsymbol{K}_{\mathrm{q}}^{-1}(\boldsymbol{p}_{\mathrm{d}}(K_{\mathrm{d}}))\hat{\boldsymbol{f}}_{\mathrm{m}}^{-1}\frac{\partial \boldsymbol{p}_{\mathrm{d}}(K_{\mathrm{d}})}{\partial \dot{\boldsymbol{x}}}\right|. \tag{41}$$

The permissible and optimal equivalent average stiffness along a desired sinusoidal trajectory (amplitude $\theta_x = 5°$ and $\theta_y = 4°$, period 20 s) are shown in Fig. 3. And Fig. 4 shows the relation between J_{opt} and K_{d} at different posture points in the process of tracking the trajectory. It can be seen from Fig. 4

that the objective function near the optimal equivalent average stiffness changes mildly, which indicates that the slight change of equivalent average stiffness in the small neighborhood of the optimal equivalent average stiffness will have slight change on reducing control input chattering. Therefore, the optimal value in practice can be a smaller constant value than the averaged value of the optimal equivalent average stiffness along certain trajectory to decrease air consumption, and consequently, save energy.

E. Some Issues on Posture Control With Redundant DOF

Remark (i). The posture controller of the PMDPM with redundancy could be flexibly designed. Besides the ARC adopted in this paper, other control methods such as PID, adaptive control, sliding-mode control, or deterministic robust control can also be used to obtain the desired drive moment. And then, the equivalent average-stiffness-like desired constraint according to different requirements is integrated into the posture controller for effectively improving tracking accuracy or reducing control input chattering.

Remark (ii). Only the value of equivalent average stiffness utilized by the controller is almost invariant in the aforementioned sinusoidal trajectory, while the equivalent stiffness around x-and y-axes fluctuate, respectively, due to the posture variations.

Remark (iii). The desired pressure vector $\boldsymbol{p}_{\mathrm{d}}$ can also be obtained from (9):

$$\boldsymbol{p}_{\mathrm{d}} = \boldsymbol{f}_{\tau}^{+}(\boldsymbol{x})(\boldsymbol{\tau}_{\mathrm{d}} - \boldsymbol{g}_{\tau}) + [\boldsymbol{I}_{3\times 3} - \boldsymbol{f}_{\tau}^{+}(\boldsymbol{x})\boldsymbol{f}_{\tau}(\boldsymbol{x})]\boldsymbol{p}_0 \quad (42)$$

where $\boldsymbol{p}_0$ is called as the equivalent average pressure vector, which is related to the equivalent average stiffness and an arbitrary 3×1 vector within the permissible range.

Substitute this $\boldsymbol{p}_{\mathrm{d}}$ as $\boldsymbol{p}$ into (11), then the relation between the equivalent average pressure vector and the equivalent average stiffness becomes

$$\boldsymbol{A}_k(\boldsymbol{x})\boldsymbol{p}_0 = B_k(\boldsymbol{x}, K_{\mathrm{d}}) \quad (43)$$

where $\boldsymbol{A}_k(\boldsymbol{x}) = \boldsymbol{f}_k(\boldsymbol{x})[\boldsymbol{I}_{3\times 3} - \boldsymbol{f}_{\tau}^{+}(\boldsymbol{x})\boldsymbol{f}_{\tau}(\boldsymbol{x})]$, $B_k(\boldsymbol{x}, K_{\mathrm{d}}) = K_{\mathrm{d}} - g_k(\boldsymbol{x}) - \boldsymbol{f}_k(\boldsymbol{x})\boldsymbol{f}_{\tau}^{+}(\boldsymbol{x})(\boldsymbol{\tau}_{\mathrm{d}} - \boldsymbol{g}_{\tau})$ in which $\boldsymbol{f}_{\tau}^{+}(\boldsymbol{x})$ is the pseudoinverse of $\boldsymbol{f}_{\tau}(\boldsymbol{x})$.

As can be seen from (43), the equivalent average stiffness corresponds to multivalued vector $\boldsymbol{p}_0$. If three components of the vector $\boldsymbol{p}_0$ are set to the same value represented by the equivalent average pressure scalar $\bar{p}_0$, a unique mapping between the equivalent average stiffness K_{d} and the equivalent average pressure scalar $\bar{p}_0$ will be established. Generally, the methods of adjusting equivalent average stiffness and regulating equivalent average pressure scalar almost have the same effects on control performance, but the method of regulating equivalent average pressure scalar is simple and explicit when applied in the posture control of the PMDPM with redundancy. In addition, it is noted that the equivalent average pressure scalar of the PMDPM takes the similar function as the average pressure scalar of antagonistic pneumatic muscle systems mentioned in previous literature [5]–[7].

Fig. 5. Experimental test rig of the PMDPM.

IV. Experimental Results

The experimental test rig shown in Fig. 5 is used to evaluate the effectiveness of the proposed posture controller with the constraint of the equivalent average stiffness. Three pneumatic muscles used in experiments are fluidic muscles manufactured by Festo, Inc. The geometric parameters of the PMDPM in Fig. 1 are $r = 0.2$ m, $R = 0.23$ m, and $h = 1.05$ m. And the rotational inertia matrix of the moving platform is $\boldsymbol{I} = \mathrm{diag}([0.457, 0.457, 0.864]^{\mathrm{T}})$. The experiments are conducted with the supply pressure 0.48 MPa. The online estimated parameters are $\boldsymbol{\beta}_{\mathrm{t}} = \boldsymbol{d}_{\mathrm{t}0}$ and $\boldsymbol{\beta}_{\mathrm{m}} = \boldsymbol{d}_{\mathrm{m}0}$ since their values have vital influences on improving model accuracy and the rest parameters are preset offline. Especially, friction force in (8) is neglected and the model error is lumped into uncertain nonlinearities. Feedback gain matrices are $\boldsymbol{K}_1 = \mathrm{diag}([80, 80]^{\mathrm{T}})$, $\boldsymbol{K}_2 = \mathrm{diag}([30, 30]^{\mathrm{T}})$, and $\boldsymbol{K}_3 = \mathrm{diag}([5, 5, 5]^{\mathrm{T}})$. And adaptation gain matrices are $\boldsymbol{\Gamma}_2 = \mathrm{diag}([70, 70]^{\mathrm{T}})$ and $\boldsymbol{\Gamma}_3 = \mathrm{diag}([5, 5, 5]^{\mathrm{T}})$.

The controller of the PMDPM is first tested for tracking a sinusoidal desired posture trajectory with amplitude $\theta_x = 5^{\circ}$, $\theta_y = 4^{\circ}$, and period 20 s under the same conditions except different constant equivalent average stiffness shown in Fig. 6–8. As can be seen, larger equivalent average stiffness of the PMDPM requires higher inner pressures of pneumatic muscles and larger control efforts while resulting in smaller control input chattering. Due to the larger time-varying friction forces caused by larger pressures, the tracking errors increase slightly under larger equivalent average stiffness. On the contrary, smaller equivalent average stiffness results in lower inner pressures of pneumatic muscles and smaller control efforts while brings much more control input chattering due to the system's sensitivity to disturbances and measurement noise under lower pressures. It is especially noted that the optimal equivalent average stiffness only used in Fig. 7 greatly reduces control input chattering and saves energy while the tracking errors are as small as those of Figs. 6 and 8.

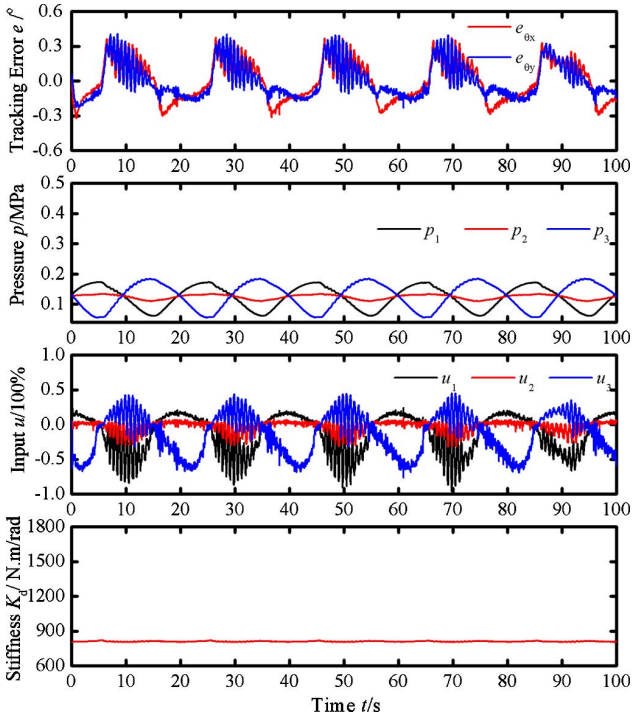

Fig. 6. Sinusoidal tracking results with $K_{\mathrm{d}} = 800\ \mathrm{N \cdot m/rad}$.

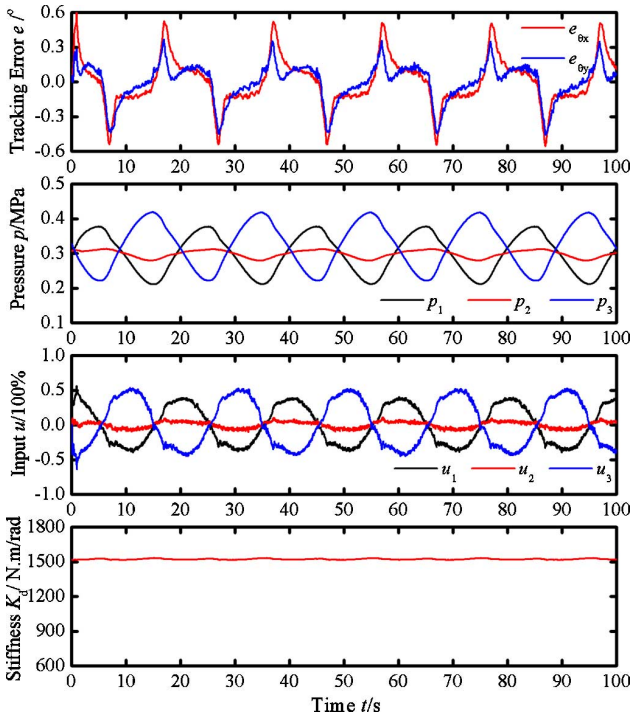

Fig. 7. Sinusoidal tracking results with $K_{\mathrm{d}} = 1500\ \mathrm{N \cdot m/rad}$.

The experimental result of time-varying equivalent average stiffness is shown in Fig. 9 under the condition of tracking the same trajectory as before. As can be seen, the time-varying equivalent average stiffness has slight influences on tracking errors during the control process. In other words, the added equivalent average-stiffness-like desired constraint has slight influences on the tracking accuracy of posture control.

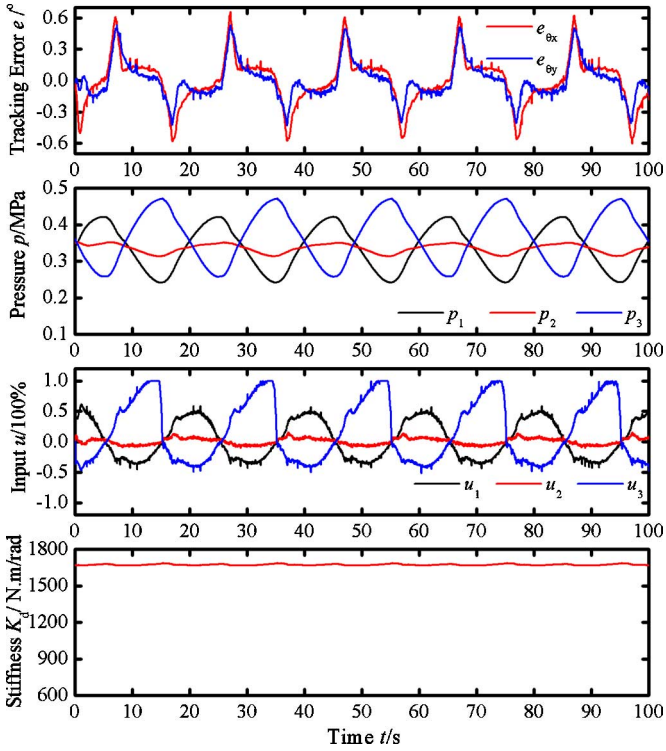

Fig. 8. Sinusoidal tracking results with $K_{\mathrm{d}} = 1650\ \mathrm{N \cdot m/rad}$.

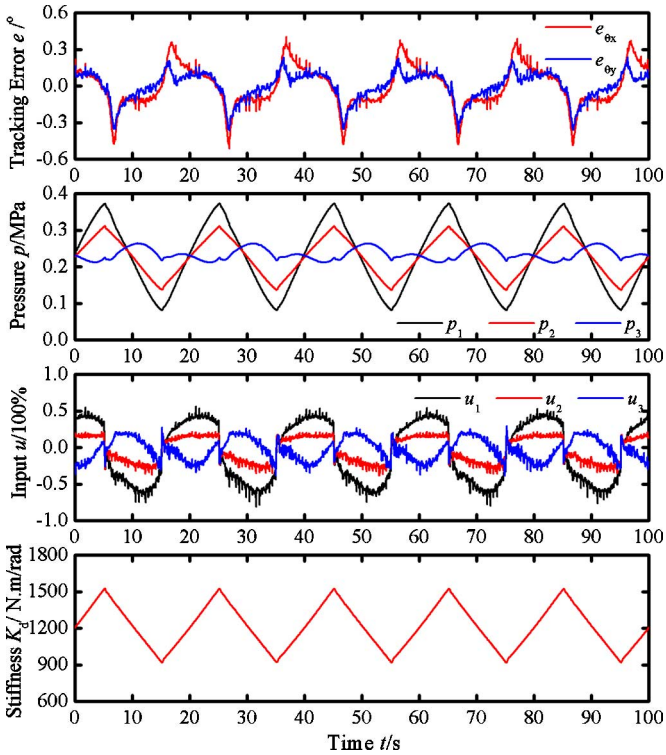

Fig. 9. Sinusoidal tracking results with time-varying K_{d}.

To sum up, all results prove the original intention that the adaptive robust posture controller with equivalent average-stiffness-like desired constraint for the PMDPM with redundancy could not only achieve small tracking errors but also reduce control input chattering.

V. Conclusion

The adaptive robust posture control with adjustable equivalent average stiffness as a constraint is proposed for precise planar posture tracking control of a parallel manipulator driven by three pneumatic muscles with a redundant design freedom. The equivalent average stiffness can be adjusted to reduce control input chattering caused by measurement noise. An adaptive robust posture controller has been developed to effectively deal with the model uncertainties existing in the complex dynamics of such a system due to factors such as time-varying friction forces, the large extent of modeling errors of pneumatic muscles, and the strong coupling and inherent nonlinearities of the parallel manipulator dynamics. Meanwhile, to make full use of the added design freedom of not controlling rotation angle around the symmetry axis of parallel manipulator, the equivalent average stiffness is introduced and its optimal value is determined to achieve the secondary objective of reducing control input chattering caused by measurement noise. Furthermore, the principle of selecting the equivalent average stiffness, the inherent characteristic of using equivalent average stiffness and equivalent average pressure scalar are discussed to provide instructions in application. Comparative experimental results are presented to illustrate the proposed control strategy as well.

Acknowledgment

The authors would like to thank the Festo(China) Ltd. for donating pneumatic components used in experiments.

References

[1] S. Davis and D. G. Caldwell, "Braid effects on contractile range and friction modeling in pneumatic muscle actuators," *Int. J. Robot. Res.*, vol. 25, no. 4, pp. 359–369, 2006.

[2] G. L. Tao, X. C. Zhu, and J. Cao, "Modeling and controlling of parallel manipulator joint driven by pneumatic muscles," *Chin. J. Mech. Eng. (English Edition)*, vol. 18, no. 4, pp. 537–541, 2005.

[3] X. C. Zhu, G. L. Tao, J. Cao, and B. Yao, "Adaptive robust posture control of a pneumatic muscles driven parallel manipulator," in *Proc. 4th IFAC Symp. Mechatron. Syst.*, Heidelberg, Germany, Sep. 12–14, 2006, pp. 764–769.

[4] L. M. Sui, Z. W. Wang, and G. Bao, "Analysis of stiffness characteristics of the pneumatic muscle actuator," *China Mech. Eng.*, vol. 15, no. 3, pp. 242–244, 2004.

[5] B. Tondu and P. Lopez, "The McKibben muscle and its use in actuating robot-arms showing similarities with human arm behaviour," *Ind. Robot*, vol. 24, no. 6, pp. 432–439, 1997.

[6] R. Liu, "On the compliant control of parallel mechanism and actuating with artificial muscle," Ph.D. dissertation, Beijing Univ. Aeronaut. Astronaut., Beijing, China, 1996.

[7] G. H. Zong and R. Liu, "On the implementation of stiffness control on a manipulator using rubber actuators," in *Proc. IEEE Int. Conf. Syst., Man Cybern. Part 1*, Vancouver, BC, Canada, Oct. 22–25, 1995, pp. 183–188.

[8] G. Tonietti and A. Bicchi, "Adaptive simultaneous position and stiffness control for a soft robot arm," in *Proc. IEEE/RSJ Int. Conf. Intell. Robots Syst.*, Lausanne, Switzerland, Sep. 30–Oct. 4, 2002, pp. 1992–1997.

[9] R. Q. van der Linde, "Design, analysis, and control of a low power joint for walking robots by phasic activation of McKibben muscles," *IEEE Trans. Robot. Autom.*, vol. 15, no. 4, pp. 599–604, Aug. 1999.

[10] A. Hildebrandt, O. Sawodny, R. Neumann, and A. Hartmann, "Cascaded control concept of a robot with two degrees of freedom driven by four artificial pneumatic muscle actuators," in *Proc. Amer. Control Conf.*, Portland, OR, Jun. 8–10, 2005, pp. 680–685.

[11] S. Liu and B. Yao, "Automated onboard modeling of cartridge valve flow mapping," *IEEE/ASME Trans. Mechatronics*, vol. 11, no. 4, pp. 381–388, Aug. 2006.

[12] Y. Hong and B. Yao, "A globally stable high-performance adaptive robust control algorithm with input saturation for precision motion control of linear motor drive systems," *IEEE/ASME Trans. Mechatronics*, vol. 12, no. 2, pp. 198–207, Apr. 2007.

[13] B. Yao and M. Tomizuka, "Adaptive robust control of SISO nonlinear systems in a semi-strict feedback form," *Automatica*, vol. 33, no. 5, pp. 893–900, 1997.

[14] B. Tondu and P. Lopez, "Modeling and control of McKibben artificial muscle robot actuators," *IEEE Control Syst. Mag.*, vol. 20, no. 2, pp. 15–38, Apr. 2000.

[15] C. P. Chou and B. Hannaford, "Measurement and modeling of McKibben pneumatic artificial muscles," *IEEE Trans. Robot. Autom.*, vol. 12, no. 1, pp. 90–102, Feb. 1996.

[16] A. Ilchmann, O. Sawodny, and S. Trenn, "Pneumatic cylinders: Modelling and feedback force control," *Int. J. Control*, vol. 79, no. 6, pp. 650–661, 2006.

[17] A. B. K. Rao, S. K. Saha, and P. V. M. Rao, "Stiffness analysis of hexaslide machine tools," *Adv. Robot.*, vol. 19, no. 6, pp. 671–693, 2005.

[18] H. K. Khalil, *Nonlinear Systems*, 2nd ed. Englewood Cliffs, NJ: Prentice-Hall, 1996.

Xiaocong Zhu received the B.Eng. and Ph.D. degrees in mechanical engineering from Zhejiang University, Hangzhou, China, in 2002 and 2007, respectively.

She is currently a Postdoctoral Fellow in the State Key Laboratory of Fluid Power Transmission and Control, Zhejiang University. Her current research interests include pneumatic servo control, nonlinear control theory and applications, mechatronic control, etc.

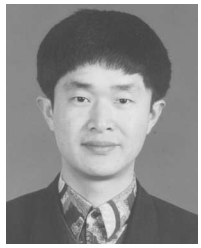

Guoliang Tao received the B.Eng., M.Eng., and Ph.D. degrees in mechanical engineering from Zhejiang University, Hangzhou, China, in 1985, 1991, and 2000, respectively.

Since 1991, he has been with the State Key Laboratory of Fluid Power Transmission and Control, Zhejiang University, where he was promoted to an Associate Researcher in 1997 and a Professor in 2001. His current research interests include nonlinear control theory and applications, mechatronic control, fluid power transmission and control, especially pneumatic servo control, and novel pneumatic components.

Bin Yao (S'92–M'96) received the B.Eng. degree in applied mechanics from Beijing University of Aeronautics and Astronautics, Beijing, China, in 1987, the M.Eng. degree in electrical engineering from Nanyang Technological University, Singapore, in 1992, and the Ph.D. degree in mechanical engineering from the University of California, Berkeley, in 1996.

Since 1996, he has been with the School of Mechanical Engineering, Purdue University, Lafayette, IN, where he was promoted to an Associate Professor in 2002 and a Full Professor in 2007. He is also one of the Kuang-Piu Professors at Zhejiang University, Hangzhou, China. His current research interests include the design and control of intelligent high-performance coordinated control of electromechanical/hydraulic systems, optimal adaptive and robust control, nonlinear observer design and neural networks for virtual sensing, modeling, fault detection, diagnostics, and adaptive fault-tolerant control, and data fusion. He is currently an Associate Editor of the *ASME Journal of Dynamic Systems, Measurement, and Control*.

Prof. Yao has been a member of various technical professional societies such as the American Society of Mechanical Engineers (ASME). He was the Organizer/Chair of numerous sessions and a member of the International Program Committee of a number of conferences of the IEEE, ASME, and the International Federation of Automatic Control (IFAC). He was the Chair of the Adaptive and Optimal Control Panel from 2000 to 2002 and the Chair of the Fluid Control Panel of the ASME Dynamic Systems and Control Division

(DSCD) from 2001 to 2003, and is currently the Vice Chair of the Mechatronics Technical Committee of the ASME DSCD that he initiated in 2005. He was a Technical Editor of the IEEE/ASME TRANSACTIONS ON MECHATRONICS from 2001 to 2005. He was a recipient of the Faculty Early Career Development (CAREER) Award from the National Science Foundation (NSF) in 1998 for his work on the engineering synthesis of high-performance adaptive robust controllers for mechanical systems and manufacturing processes, a Joint Research Fund for Overseas Young Scholars from the National Natural Science Foundation of China (NSFC) in 2005, and the O. Hugo Schuck Best Paper (Theory) Award from the American Automatic Control Council in 2004.

Jian Cao received the B.Eng. degree in fluid power transmission and control from the Inner Mongolia University of Science and Technology, Baotou, China, in 2002. He is currently working toward the Ph.D. degree in mechanical engineering at the State Key Laboratory of Fluid Power Transmission and Control, Zhejiang University, Hangzhou, China.

His current research interests include fluid power transmission and control, mechatronic control, etc.